Cellulose (2019) 26:8279–8290
https://doi.org/10.1007/s10570-019-02466-1

ORIGINAL RESEARCH

Insight into the mechanism of secondary reactions in cellulose pyrolysis: interactions between levoglucosan and acetic acid

Qiang Lu · Yu-ting Wu · Bin Hu · Ji Liu · Ding-jia Liu · Chang-qing Dong · Yong-ping Yang

Received: 12 January 2019 / Accepted: 29 April 2019 / Published online: 6 May 2019

Abstract Biomass pyrolysis process involves complex primary and secondary decomposition reactions which together determine the final pyrolytic product distribution. Carboxylic acids produced by primary pyrolysis have significant influences on the secondary reactions, whereas the specific manifestation of these influences has not been determined. In this work, acetic acid (AA) and levoglucosan (LG) are selected as the research objects to explore the influence of carboxylic acids on secondary pyrolysis process, considering AA is usually the most abundant carboxylic acid product, while LG is the major depolymerization product of cellulose as well as the representative of polyhydroxy compounds. The interaction mechanisms between them are investigated by density functional theory calculation. The results indicate that there are four types of important interactions between AA and LG, namely esterification reactions, organic redox reactions, AA-catalyzed LG dehydration reactions, LG-catalyzed AA decomposition reactions. These interaction reactions are more competitive than the unimolecular decomposition reactions of AA and LG. Moreover, AA-catalyzed dehydration reactions dominate interaction reactions.

Electronic supplementary material The online version of this article (https://doi.org/10.1007/s10570-019-02466-1) contains supplementary material, which is available to authorized users.

Q. Lu (✉) · Y. Wu · B. Hu · J. Liu · D. Liu · C. Dong · Y. Yang
National Engineering Laboratory for Biomass Power Generation Equipment, North China Electric Power University, Beijing 102206, China
e-mail: qianglu@mail.ustc.edu.cn; qlu@ncepu.edu.cn

Graphical abstract

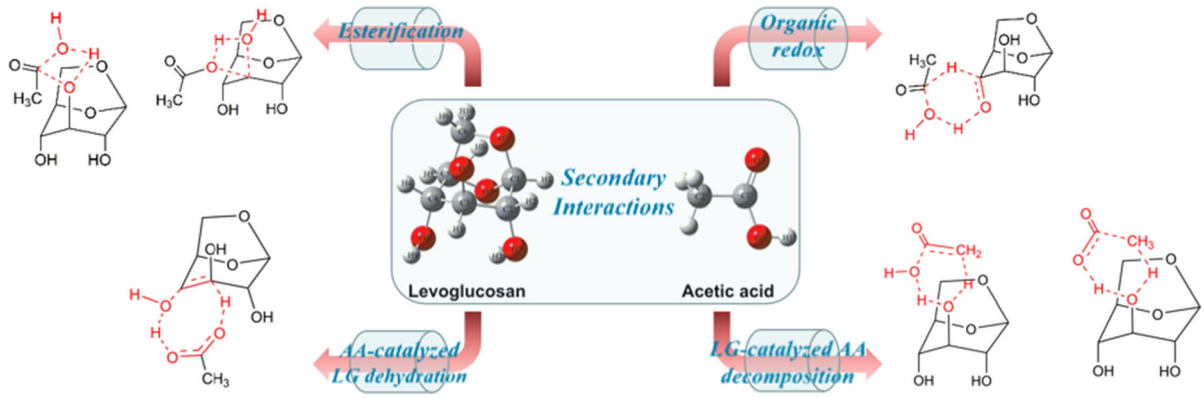

Keywords Cellulose · Pyrolysis · Secondary reactions · Interaction mechanism · Acetic acid · Levoglucosan

Introduction

Lignocellulosic biomass is an important renewable resource in the energy and chemical industries (Hausser et al. 2013; Sacchelli et al. 2013; Loow et al. 2016; Ozturk et al. 2017). Pyrolysis has been recognized as an effective and promising technique to convert raw biomass materials into valuable solid, liquid and gaseous products under specific conditions (Williams and Besler 1996; Jahirul et al. 2012). During the pyrolysis process, the primary pyrolytic products from biomass decomposition will further undergo secondary reactions to form the final products. Both primary and secondary pyrolysis reactions occur in a very short time without clear boundaries (Kan et al. 2016). Typically, when the residence time of pyrolytic vapors is particularly short, the occurrence of secondary reactions can be ignored. While at long residence time or high pyrolysis temperatures, secondary reactions show fundamental influences on the whole pyrolysis process (Bridgwater 1999; Fisher et al. 2002).

During biomass fast pyrolysis process, the primary decomposition produces various anhydrosugars [dominated by levoglucosan (LG)], furan derivatives, linear carbonyls, carboxylic acids [dominated by acetic acid (AA)], phenolics, and so on (Adam et al. 2005; Lu et al. 2011a, b; Mihalcik et al. 2011). The secondary cracking of primary products has been investigated (Mackie and Doolan 1984; Nguyen et al. 1995; Nimlos and Evans 2002; Zhang et al. 2012, 2013; Fukutome et al. 2017), mainly focusing on the unimolecular decomposition reactions. LG is the typical depolymerization product of cellulose and usually the most abundant anhydrosugar product in biomass primary pyrolysis process (Lu et al. 2011b). It has been proposed that at high temperatures, gaseous LG can selectively fragment into small molecule aldehydes/ketones (such as glyoxal or formaldehyde) and non-condensable gases (Fukutome et al. 2015, 2017). Based on a pyrolysis experiment of LG in a two-stage alumina tubular reactor under argon atmosphere, Nimlos and Evans (2002) found that LG was first converted into dehydrated LG, carbonylated LG and 3,6-anhydro-D-glucose through the C–O ether bond cleavage and synergistic dehydration. Subsequently, these products were decomposed into small molecular products such as 2,3-butanedione, pyruvic aldehyde, acetaldehyde, etc.

In addition to the unimolecular decompositions of primary pyrolysis products, interactions between different primary products are also important for the distribution of final products. Previous studies have revealed that carboxylic acids from the primary pyrolysis process showed remarkable effects on the secondary pyrolysis process (Hosoya et al. 2007; Shen and Gu 2009; Patwardhan et al. 2011). AA is the dominant carboxylic acid product which derives from all the three major components of biomass (Patwardhan et al. 2009; Nowakowski et al. 2010; Oasmaa et al. 2010), especially from the deacetylation of hemicellulose (Shen et al. 2010, 2015; Wang et al. 2015).

Carrier et al. (2017) investigated the composition differences of bio-oils derived from different individual biopolymers including cellulose, hemicellulose, and lignin extracted from Zea Mays. Obviously, hemicellulose-derived bio-oil was found to contain the highest acids (8.56 wt%) mainly consisting of short-chain acids like AA and propionic acid. Meng et al. (2016) performed fast pyrolysis experiments of cellulose impregnated with 10 wt% AA solution at 623 K. Results indicated that the yields of anhydrosugars [levoglucosenone (LGO), 1,4:3,6-dianhydro-α-D-glucopyranose (DGP), and 1,6-anhydro-β-D-glucofuranose (AGF)] increased, particularly for AGF, suggesting that AA could enhance the dehydration reactions in pyrolysis. In addition, Mamleev et al. (2009) proposed that volatile acids like AA dissolved in the liquid were strong catalysts to accelerate various heterolytic (ionic) reactions, such as depolymerization by the acid-catalyzed β-elimination.

The previous studies verified that carboxylic acids played an important role in biomass fast pyrolysis. However, little experimental or theoretical research has been reported on the mechanisms of secondary interaction reactions between carboxylic acids and other primary products at present. Compared with experimental methods, the theoretical calculation to investigate the fast pyrolysis mechanisms of biomass or its components should employ simplified model compounds, which leads to an obvious gap between theoretical and actual pyrolysis mechanisms. However, due to the difficulties of strictly controlling the reaction process and identifying the intermediates in experimental research, theoretical calculation methods are very important for investigating the detailed mechanisms of complex biomass or individual biopolymers pyrolysis. For example, glucose, xylose, and phenols are often used as model compounds to study the thermal degradation mechanisms of cellulose, hemicellulose, and lignin, respectively (Wang et al. 2012; Huang et al. 2013; Zhang et al. 2015; Huang et al. 2016). In this work, based on quantum chemistry calculation method, AA and LG were selected as the research models to investigate the mechanisms of secondary reactions involved in the cellulose fast pyrolysis process at the micro level. Both unimolecular and bimolecular decomposition of AA and LG were studied. The theoretical results were also compared with reported experimental results to confirm the feasibility and reliability.

Computational details

In this study, the most stable configuration of LG ($^1C_4$ configuration) reported by Hosoya et al. (2009) and Kabo et al. (2015) was employed and optimized at B3LYP/6-311G(d,p) level for further investigation. The structures and atomic labels of LG and AA are shown in Fig. 1. The key structural parameters of LG and AA are listed in Table 1, including the bond lengths, bond angles and dihedral angles.

All the calculations were performed at 298 K based on density functional theory (DFT) by using Gaussian 09 software package (Frisch et al. 2013). The selected functional and basis set were classical hybrid functional B3LYP and the 3-zeta basis set 6-311G(d,p) with polarization functions added to the heavy atoms and light atoms, respectively. Unrestricted geometric optimizations were performed firstly on all initial guess structures to find the minimum points of the potential energy surface in the system. Then the vibration analyses of optimized geometries were performed at the same calculation level (Wong 1996). Considering that DFT cannot well describe the dispersion effect, zero-damping DFT-D3 dispersion correction was employed (Grimme et al. 2010). All reactants and products were local minimum points on the potential energy surface without imaginary frequencies. Each transition state was the first-order saddle point on the potential energy surface with only one imaginary frequency. The intrinsic reaction coordinate (IRC) analysis was carried out to further judge whether the transition state was correctly connected to the minimum points on the potential energy surface (Gonzalez and Schlegel 1990). All energies in the study were subjected to zero-point energy (ZPE) correction, and the relative energy difference between the transition state and the reactants was used to estimate the reaction energy barrier. Optimized geometries and atom coordinates for all compounds are shown in the electronic supplementary material.

In addition, KiSThelP program (Canneaux et al. 2014) was used to calculate the reaction rate constants of bimolecular interactions at different temperatures based on the transition state theory. The unit of reaction rate constant k is s^{-1} M^{-1}. The reaction path degeneracy was set to 1 (default) and the resonance frequency correction factor was set to 0.98. The frequency analysis files calculated by Gaussian 09 were used as input files for the KiSThelP program, and

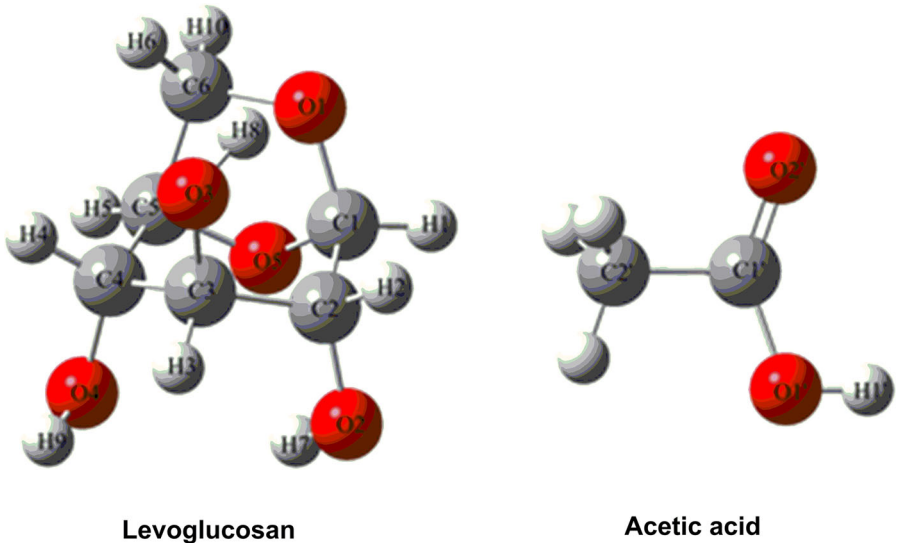

Fig. 1 Optimized geometries of LG and AA at B3LYP/6-311G(d,p) level (gray ball: C, red ball: O, white ball: H). (Color figure online)

Table 1 Key structural parameters of optimized geometries of LG and AA

Key structural parameters			
Bond length (Å)			
C_1–C_2	1.541	C_5–O_5	1.439
C_2–C_3	1.546	O_4–H_7	2.365
C_3–C_4	1.554	O_5–H_7	2.359
C_4–C_5	1.534	O_1-H_8	2.050
C_5–C_6	1.529	C_1'–C_2'	1.506
C_1–O_1	1.443	C_1'–O_1'	1.358
C_6–O_1	1.447	C_1'–O_2'	1.203
C_1–O_5	1.412		
Bond angle (°)			
C_1–O_5–C_5	102.386	C_4–C_5–O_5	109.512
C_1–O_1–C_6	106.603	C_2'–C_1'–O_2'	126.192
C_2–C_1–O_5	108.349	C_2'–C_1'–O_1'	111.117
C_2–C_3–C_4	110.409		
Dihedral angle (°)			
C_1–O_5–C_4–C_5	111.016	C_4–O_5–C_5–C_6	119.63
C_2–C_3–C_1–O_5	120.555	C_5–O_5–C_6–O_1	14.377
C_3–C_1–C_4–O_3	33.446		

different pyrolysis temperatures were set in the program to obtain reaction rate constants of all interactions at different temperatures. Based on these data, it was able to draw the curves of reaction rate constants along with temperatures, as shown in Figs. S2–S5 of the supplementary material.

Results and discussion

Unimolecular decompositions of LG and AA

The unimolecular decomposition of LG has been investigated via both experimental methods and computational calculations in previous studies (Zhang et al. 2012, 2013; Fukutome et al. 2017). Based on these results, it can be concluded that the main unimolecular decomposition reactions of LG include 1,2-dehydration reactions, 1,3-dehydration reactions, and ring-opening reactions. The detailed reaction pathways are calculated in this work, as shown in Fig. 2a.

According to LG structure, the three hydroxyl groups on the LG molecule have different spatial orientations. These hydroxyl groups can undergo 1,2-dehydration reactions with hydrogen atoms on adjacent carbon atoms to form various dehydrated LG products (P1–P6), as shown in Reactions 1–6. In addition, two hydroxyl groups of LG molecule in the meta position can undergo 1,3-dehydration reactions which cause partial ring-opening of LG, as shown in Reactions 8 and 9. Besides, LG can also undergo ring-opening reaction (Reaction 7) where C_1–O bond and C_6-O bond are broken accompanied by hydrogen-shift between C_5 and C_6 to form the acyclic product 5-keto-

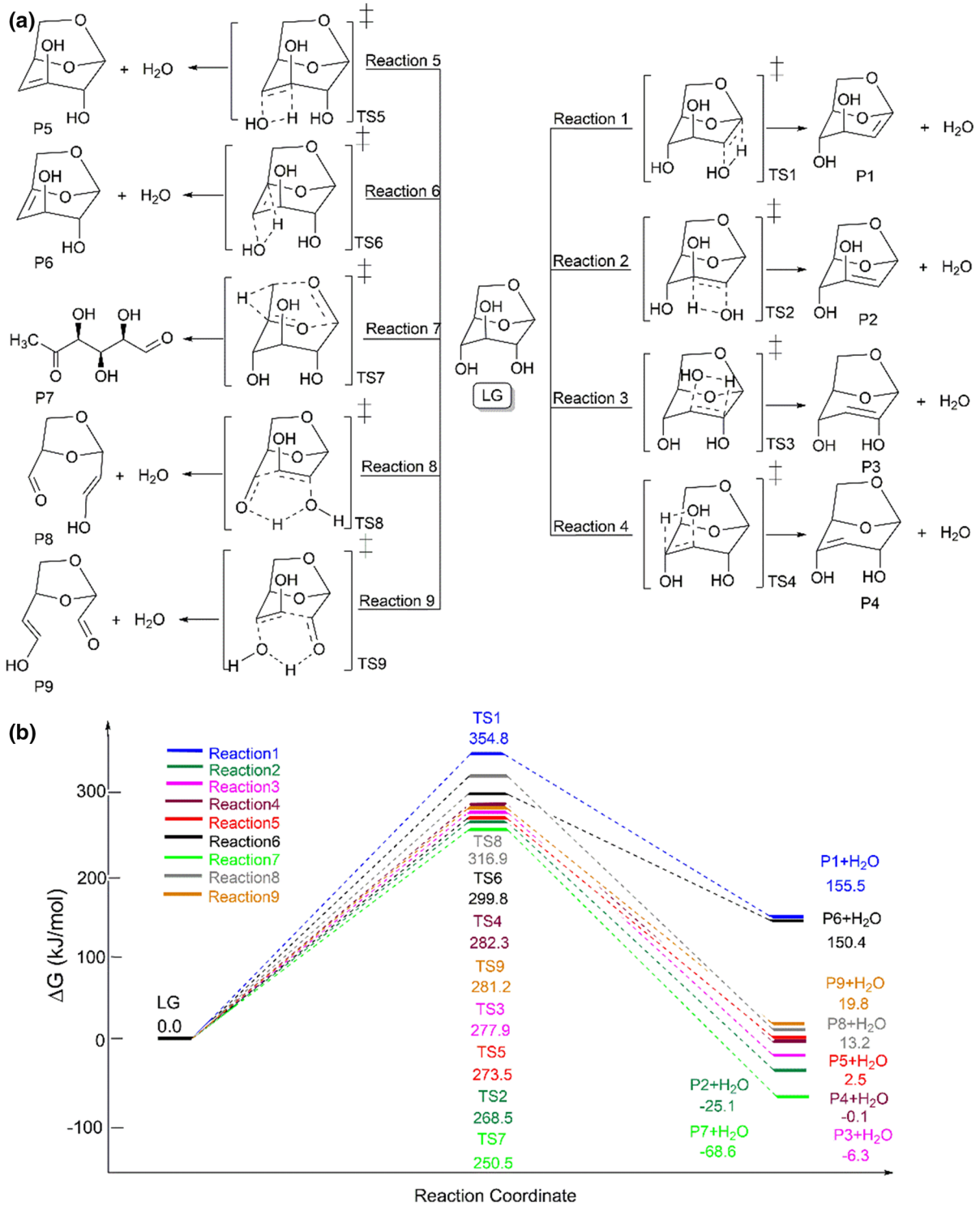

Fig. 2 Unimolecular decomposition reactions of LG. **a** Reaction pathways; **b** reaction energy barriers

6-deoxy-glucose (P7). The activation free energies (ΔG) of the transition states and products are calculated as shown in Fig. 2b. According to the energy diagram, the dominant reaction in the LG unimolecular decomposition is Reaction 7.

In regard to AA, its main decomposition reactions include decarboxylation reactions and dehydration reactions (Mackie and Doolan 1984; Nguyen et al. 1995). The detailed reaction pathways are shown in Fig. 3a. In the decarboxylation reaction (Reaction 10), the hydrogen on the carboxyl group of AA is transferred to the methyl carbon position. Meanwhile, the C_1'–C_2' bond is broken to form CH_4 and CO_2. In Reaction 11, AA can undergo 1,2-dehydration to form water and ethenone, which is very active and easy to polymerize to form diketene or react with AA or water to form acetic anhydride or AA, respectively. The energy diagram shown in Fig. 3b implies that AA tends to undergo Reaction 10 to form CH_4 and CO_2.

Interactions between LG and AA

Based on the structural analysis of LG and AA, four types of bimolecular interactions may occur between them, namely esterification reactions, organic redox reactions, AA-catalyzed LG dehydration reactions, and LG-catalyzed AA decomposition reactions.

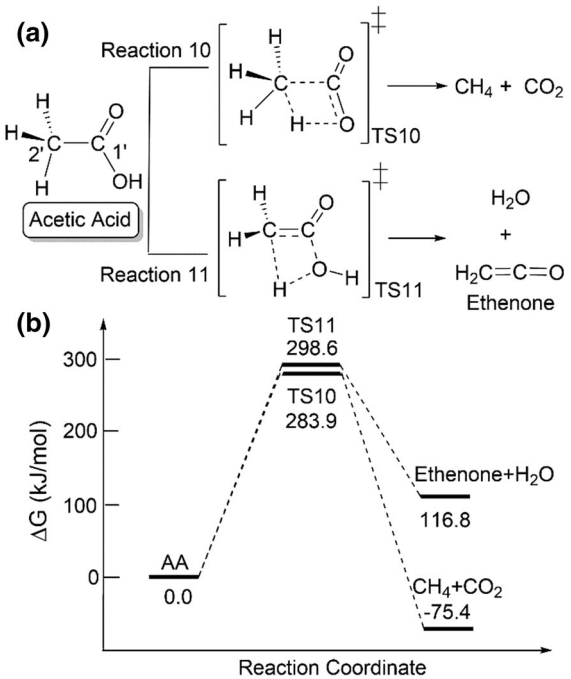

Fig. 3 Unimolecular decomposition reactions of AA. **a** Reaction pathways; **b** reaction energy barriers

Esterification reactions

The esterification reactions can be classified into two categories ("Type A" reactions and "Type B" reactions) according to the source of the hydroxyl group and the hydrogen atom in the produced water molecule, as shown in Reactions 12–17 in Fig. 4. In "Type A" reactions, AA donates the proton to the hydroxyl group of LG. Conversely, LG acts as the donator of hydrogen in "Type B" reactions. Based on the energy diagram, esterification between AA and LG tends to take place by Reaction 15 due to the relatively low energy barrier. In addition, in comparison of reactions with the same products (the same color in Fig. 4), the energy barriers of "Type B" reactions are lower than those of "Type A" reactions. This indicates that esterification reactions occurred between AA and LG are consistent with classical esterification reactions occurred in solution, namely, acids provide the hydroxyl group while alcohols provide the hydrogen.

Organic redox reactions

In organic redox reactions, LG is oxidized to a ketone structure while AA is reduced to acetaldehyde, as shown in Reactions 18–20 in Fig. 5. LG donates the hydroxyl hydrogen to the hydroxyl group on AA accompanied by the hydrogen-shift process between two related carbon atoms to form water, carbonylated LG and acetaldehyde. The energy barriers of these reactions are close to each other, with Reaction 18 possessing the lowest value, which suggests that organic redox reactions tend to occur at the C_4 position of LG.

AA-catalyzed LG dehydration reactions

Different from the above reactions, AA acts as a catalyst in the third type of interaction reactions to catalyze the dehydration of LG, as shown in Reactions 21–26 in Fig. 6. In these reactions, the carboxyl group of AA provides the hydrogen to the hydroxyl group of LG. Meanwhile, the carbonyl oxygen of AA attracts the ortho-hydrogen of the hydroxyl group on LG to form a new AA molecule. According to the energy diagram, AA is more likely to catalyze

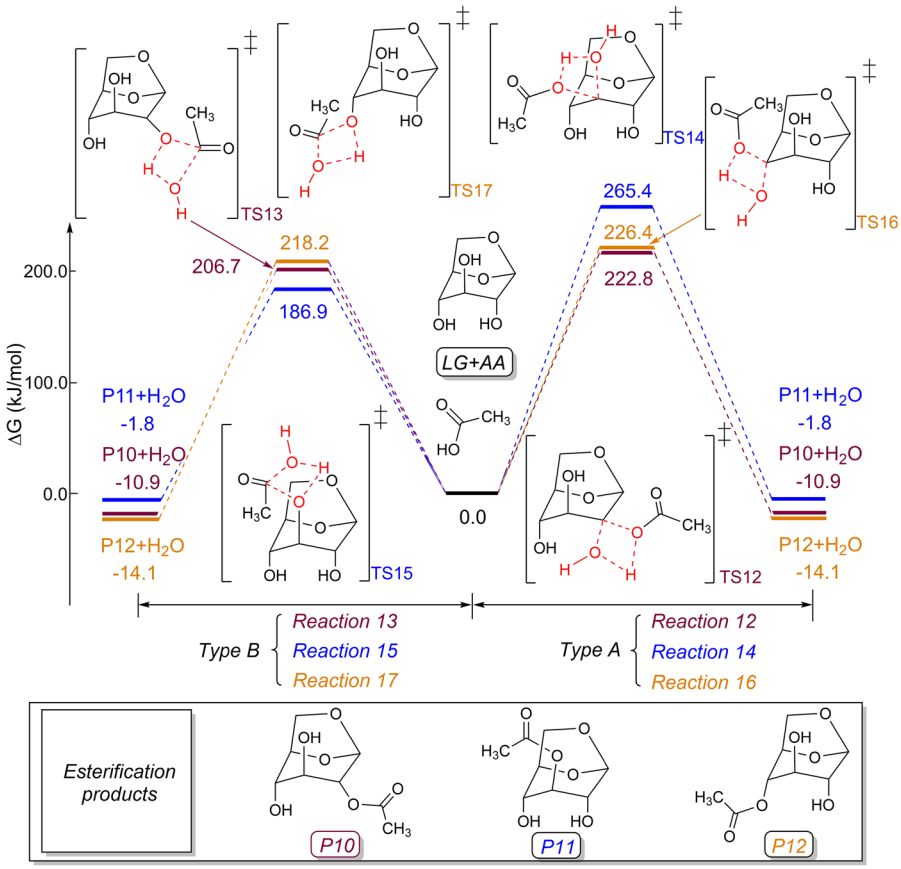

Fig. 4 Esterification reactions between LG and AA

Reaction 25 to produce the dehydrated LG with an unsaturated C_3=C_4 bond.

LG-catalyzed AA decomposition reactions

LG can also catalyze the decarboxylation and dehydration of AA, as shown in Fig. 7. In LG-catalyzed decarboxylation reactions of AA (Reactions 27–29), the hydroxyl group of LG provides a proton to the methyl group of AA to form methane, while accepting the carboxyl hydrogen provided by AA to form a new LG molecule accompanied with the formation of CO_2. Differently, in LG-catalyzed dehydration reactions of AA (Reactions 30–32), the hydroxyl group of AA reacts with the hydroxyl hydrogen of LG to form water. Meanwhile, the methyl group of AA provides a proton to LG to form a new LG molecule and ethenone. Based on the energy diagram, LG tends to catalyze the dehydration of AA to form water and ethenone rather than the decarboxylation due to the lower energy barriers.

Discussion

The energy barriers of both unimolecular decomposition reactions and bimolecular interaction reactions are summarized in Table 2, according to which the most feasible reaction in each reaction type can be easily distinguished. For LG unimolecular decomposition, the ring-opening reaction (Reaction 7) with an energy barrier of 250.5 kJ/mol is more favorable than 1,2-dehydration and 1,3-dehydration. In the case of AA unimolecular decomposition, AA is likely to undergo decarboxylation with an energy barrier of 283.9 kJ/mol to form CH_4 and CO_2. With regard to the four types of bimolecular interaction reactions, Reaction 15 is easy to take place for esterification between AA and LG due to the low energy barrier (186.9 kJ/mol) where the hydroxyl group attached to the C_3 position of LG donates the proton to the hydroxyl group of AA. In organic redox reactions, Reaction 18 (233.0 kJ/mol) is the most feasible reaction that occurs at the C_4 position of LG. In AA-

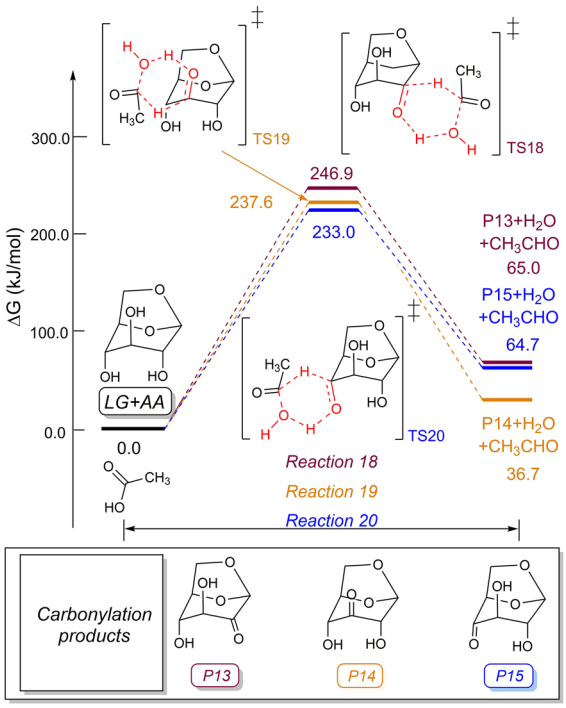

Fig. 5 Organic redox reactions between LG and AA

catalyzed LG dehydration reactions, AA is more likely to catalyze Reaction 25 to produce the dehydrated LG with an unsaturated C_3=C_4 bond overcoming an energy barrier of 177.6 kJ/mol. Different from the AA unimolecular decomposition, AA tends to undergo dehydration through Reaction 30 (210.8 kJ/mol) to form ethenone and water in LG-catalyzed AA decomposition reactions. Comparing the above energy barriers, the interaction reactions are more competitive than the unimolecular decomposition reactions, implying that these interaction reactions are feasible to occur in the secondary decomposition process.

Based on the four types of bimolecular interactions, AA and LG act not only as a reactant but also a catalyst to participate in the interactions. Obviously, the energy barrier of Reaction 25 is the lowest among all the reactions, which supports the conclusion that AA is more likely to act as a catalyst to affect the interaction reactions. The energy barriers of 1,2-dehydration reactions of LG are greatly reduced by AA. Similarly, the energy barriers of decarboxylation

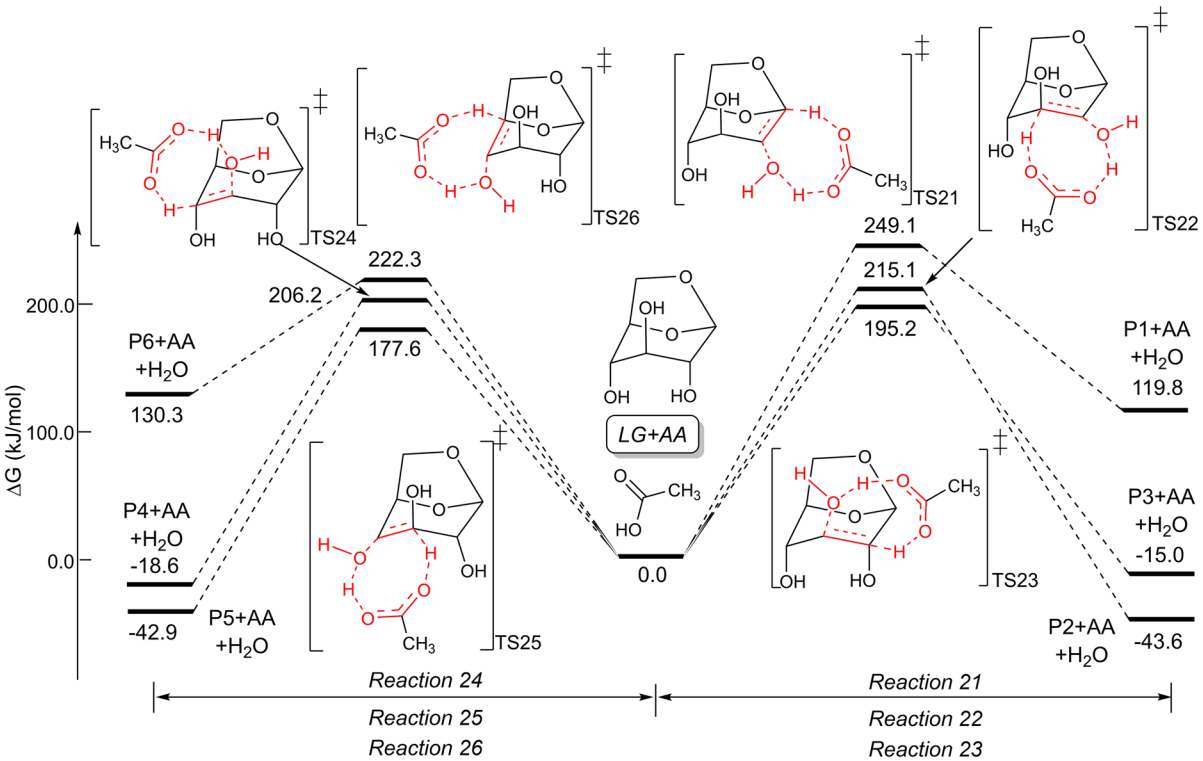

Fig. 6 AA-catalyzed LG dehydration reactions

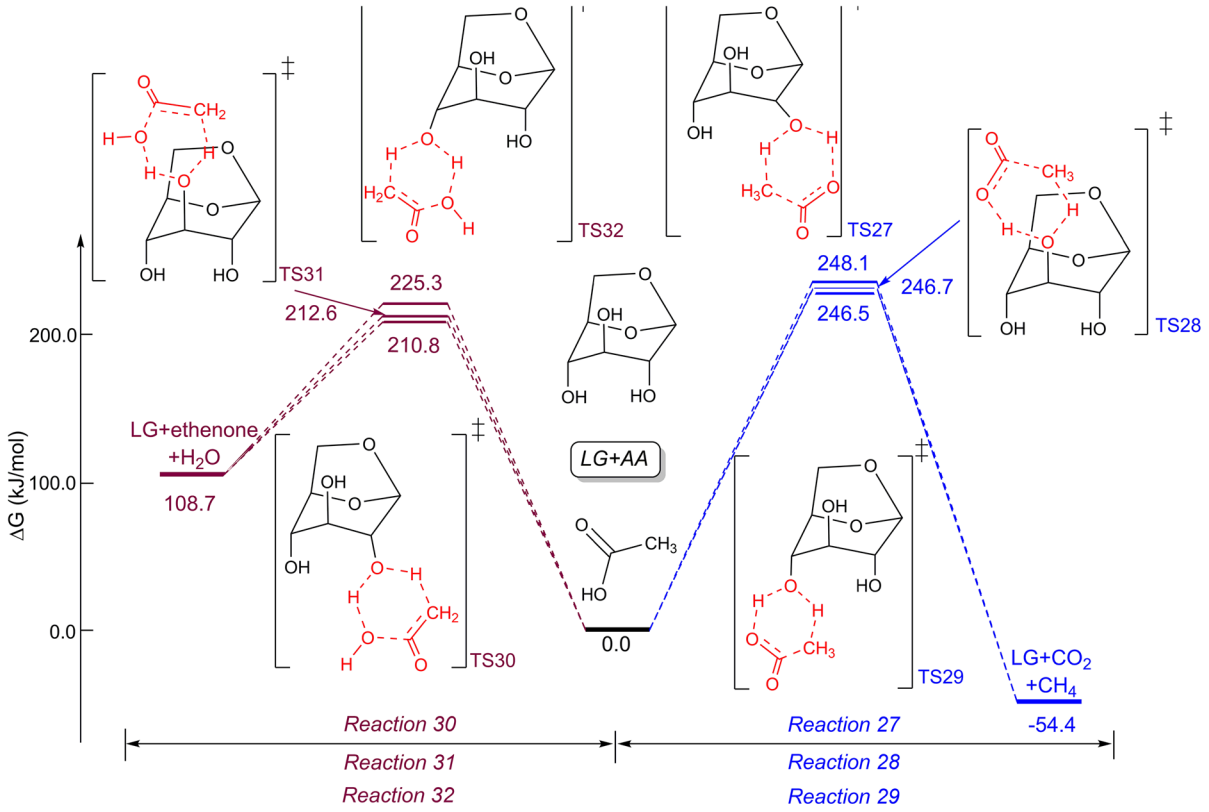

Fig. 7 LG-catalyzed AA decomposition reactions (blue for decarboxylation, brown for dehydration)

Table 2 The energy barriers of unimolecular decomposition reactions and bimolecular interaction reactions (unit: kJ/mol)

Unimolecular				Bimolecular							
LG		AA		Esterification reaction		Organic redox reaction		AA-catalyzed LG dehydration reaction		LG catalyzed AA decomposition reaction	
R1	354.8	R10	283.9	R12	222.8	R18	246.9	R21	249.1	R27	248.1
R2	268.5	R11	298.6	R13	206.7	R19	237.6	R22	215.1	R28	246.7
R3	277.9			R14	265.4	R20	233.0	R23	195.2	R29	246.5
R4	282.3			R15	186.9			R24	206.2	R30	210.8
R5	273.5			R16	226.4			R25	177.6	R31	212.6
R6	299.8			R17	218.2			R26	222.3	R32	225.3
R7	250.5										
R8	316.9										
R9	281.2										

The letter "R" represents "Reaction"

and dehydration of AA under the catalysis of LG are also reduced dramatically.

In addition to the energy barriers, the reaction rate constants of all interaction reactions at different pyrolysis temperatures (423 K, 473 K, 573 K, 673 K, 773 K, 873 K, 973 K) were also calculated, as shown in Figs. S2–S5 of the supplementary material. All bimolecular reactions are assumed to

have the same reactant concentration. Thus, the calculated reaction rate constants can represent reaction rates. It can be seen from Figs. S2–S5 that the reaction rate constants of all interaction reactions increase along with the pyrolysis temperature. The reactions with low energy barriers have large reaction rate constants. Furthermore, the reaction with the lowest energy barrier in each reaction type is taken as the typical representative to compare the reaction rate constants of four types of interactions at different temperatures, as shown in Fig. 8. When the pyrolysis temperature is lower than 473 K, the reaction rate constant of Reaction 15 is the largest, while the reaction rate constant of Reaction 25 is quite close to it. In the temperature range of 573–973 K, the reaction rate constants of Reaction 25 become the largest. Therefore, AA-catalyzed LG dehydration reactions have the highest reaction rates and the most obvious advantage in the fast pyrolysis mode (high-temperature conditions) when compared with the other three interaction types, which is consistent with the energy barrier analysis. Moreover, the reaction rate constants of Reaction 29 are the smallest at all temperatures, which indicates that LG-catalyzed AA decarboxylation reactions are slow and difficult to occur.

As mentioned above, the secondary reactions can be significantly enhanced by increasing the pyrolysis temperature or residence time of pyrolytic vapors. Patwardhan et al. (2011) experimentally investigated the differences between primary pyrolysis and secondary pyrolysis by controlling the residence time of pyrolysis vapors. The results clearly indicated that the secondary reactions significantly increased permanent gases (CO_2, CO, etc.) and water, while decreased organic products (LG, furan, 5-hydroxymethylfurfural, etc.). Whereas, only a slight change was observed in the yield of AA. The above experimental results are consistent with our calculations that AA mainly participates in the secondary pyrolysis as a catalyst. Although the decarboxylation or dehydration of AA occurs more easily under the catalysis of LG, it cannot lead to a substantial reduction in AA yield. Two possible reasons should be responsible for this result. First, in the LG-catalyzed AA decomposition process, AA tends to produce ethenone and water via dehydration rather than decarboxylation to form CH_4 and CO_2. While ethenone is chemically active that can easily react with water through 1,2-addition reaction at a high temperature to regenerate AA. Second, the secondary decomposition of primary products may also generate AA. Therefore, it is reasonable that the yield of AA is relatively stable in the pyrolysis experiment of Patwardhan et al.

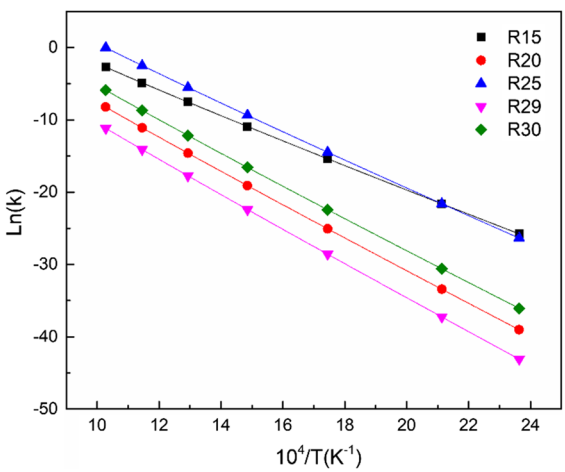

Fig. 8 Comparison of the reaction rate constants of typical bimolecular interaction reactions at different temperatures (the letter "R" represents "Reaction")

Based on the above discussion, it can be inferred that carboxylic acids play an important role in the secondary reactions of biomass. They can act as not only a reactant to participate in the unimolecular decomposition, esterification reactions or redox reactions, but also a catalyst in the dehydration of LG and other products. Moreover, they will also partially undergo decarboxylation and dehydration reactions under the catalysis of LG and other products.

Conclusions

In this work, the mechanism of secondary reactions during cellulose pyrolysis was studied by DFT calculation. AA and LG were selected as the research models to calculate and analyze their unimolecular reaction pathways as well as four types of bimolecular interaction reaction pathways including esterification reactions, organic redox reactions, AA-catalyzed LG dehydration reactions, and LG-catalyzed AA decomposition reactions. According to the energy diagrams, bimolecular interaction reactions are more competitive than the unimolecular decomposition reactions. Among the interaction reactions, AA-catalyzed LG dehydration reactions are the most feasible to occur

which is further proved to be reliable by the analysis of the calculated reaction rate constants, suggesting that AA tends to be a catalyst during the secondary decomposition process. Similarly, LG can also act as a catalyst to promote the dehydration of AA. Whereas, the dehydrated product of AA can easily regenerate into AA under pyrolysis conditions, and thus, the AA yield can remain stable during the secondary reactions. Overall, the present work provides a basic insight into the mechanism of the secondary interactions in cellulose pyrolysis, establishing the foundation for comprehensive and deep studies in the future.

Acknowledgments The authors thank the National Natural Science Foundation of China (51576064, 51821004), Beijing Nova Program (Z171100001117064), Beijing Natural Science Foundation (3172030), Grants from Fok Ying Tung Education Foundation (161051), and Fundamental Research Funds for the Central Universities (2018ZD08, 2017ZZD05) for financial support.

References

Adam J, Blazsó M, Mészáros E, Stöcker M, Nilsen MH, Bouzga A, Hustad JE, Grønli M, Øye G (2005) Pyrolysis of biomass in the presence of Al-MCM-41 type catalysts. Fuel 84(12–13):1494–1502

Bridgwater AV (1999) Principles and practice of biomass fast pyrolysis processes for liquids. J Anal Appl Pyrol 51(1–2):3–22

Canneaux S, Bohr F, Henon E (2014) KiSThelP: a program to predict thermodynamic properties and rate constants from quantum chemistry results. J Comput Chem 35(1):82–93

Carrier M, Windt M, Ziegler B, Appelt J, Saake B, Meier D, Bridgwater A (2017) Quantitative insights into the fast pyrolysis of extracted cellulose, hemicelluloses, and lignin. ChemSusChem 10(16):3212–3224

Fisher T, Hajaligol M, Waymack B, Kellogg D (2002) Pyrolysis behavior and kinetics of biomass derived materials. J Anal Appl Pyrol 62(2):331–349

Frisch MJ, Trucks GW, Schlegel HB et al (2013) Gaussian 09, Revision D. 01. Gaussian Inc., Wallingford

Fukutome A, Kawamoto H, Saka S (2015) Processes forming gas, tar, and coke in cellulose gasification from gas-phase reactions of levoglucosan as intermediate. ChemSusChem 8(13):2240–2249

Fukutome A, Kawamoto H, Saka S (2017) Kinetics and molecular mechanisms for the gas-phase degradation of levoglucosan as a cellulose gasification intermediate. J Anal Appl Pyrol 124:666–676

Gonzalez C, Schlegel HB (1990) Reaction path following in mass-weighted internal coordinates. J Phys Chem 94(14):5523–5527

Grimme S, Antony J, Ehrlich S, Krieg H (2010) A consistent and accurate ab initio parametrization of density functional dispersion correction (DFT-D) for the 94 elements H-Pu. J Chem Phys 132(15):154104

Hausser N, Marinkovic S, Estrine B (2013) New method for lignocellulosic biomass polysaccharides conversion in butanol, an efficient route for the production of butyl glycosides from wheat straw or poplar wood. Cellulose 20(5):2179–2184

Hosoya T, Kawamoto H, Saka S (2007) Pyrolysis behaviors of wood and its constituent polymers at gasification temperature. J Anal Appl Pyrol 78(2):328–336

Hosoya T, Nakao Y, Sato H, Kawamoto H, Sakaki S (2009) Thermal degradation of methyl β-D-glucoside. A theoretical study of plausible reaction mechanisms. J Org Chem 74(17):6891–6894

Huang JB, Li XS, Wu D, Tong H, Li WM (2013) Theoretical studies on pyrolysis mechanism of guaiacol as lignin model compound. J Renew Sustain Energy 5(4):043112

Huang XY, Cheng DG, Chen FQ, Zhan XL (2016) Reaction pathways of hemicellulose and mechanism of biomass pyrolysis in hydrogen plasma: a density functional theory study. Renew Energy 96:490–497

Jahirul MI, Rasul MG, Chowdhury AA, Ashwath N (2012) Biofuels production through biomass pyrolysis—a technological review. Energies 5(12):4952–5001

Kabo GJ, Paulechka YU, Voitkevich OV, Blokhin AV, Stepurko EN, Kohut SV, Voznyi YV (2015) Experimental and theoretical study of thermodynamic properties of levoglucosan. J Chem Thermodyn 85:101–110

Kan T, Strezov V, Evans TJ (2016) Lignocellulosic biomass pyrolysis: a review of product properties and effects of pyrolysis parameters. Renew Sustain Energy Rev 57:1126–1140

Loow YL, Wu TY, Jahim JM, Mohammad AW, Teoh WH (2016) Typical conversion of lignocellulosic biomass into reducing sugars using dilute acid hydrolysis and alkaline pretreatment. Cellulose 23(3):1491–1520

Lu Q, Dong CQ, Zhang XM, Tian HY, Yang YP, Zhu XF (2011a) Selective fast pyrolysis of biomass impregnated with $ZnCl_2$ to produce furfural: analytical Py–GC/MS study. J Anal Appl Pyrol 90(2):204–212

Lu Q, Yang XC, Dong CQ, Zhang ZF, Zhang XM, Zhu XF (2011b) Influence of pyrolysis temperature and time on the cellulose fast pyrolysis products: analytical Py–GC/MS study. J Anal Appl Pyrol 92(2):430–438

Mackie JC, Doolan KR (1984) High-temperature kinetics of thermal decomposition of acetic acid and its products. Int J Chem Kinet 16(5):525–541

Mamleev V, Bourbigot S, Le Bras M, Yvon J (2009) The facts and hypotheses relating to the phenomenological model of cellulose pyrolysis: interdependence of the steps. J Anal Appl Pyrol 84(1):1–17

Meng X, Zhang H, Liu C, Xiao R (2016) Comparison of acids and sulfates for producing levoglucosan and levoglucosenone by selective catalytic fast pyrolysis of cellulose using Py–GC/MS. Energy Fuel 30(10):8369–8376

Mihalcik DJ, Mullen CA, Boateng AA (2011) Screening acidic zeolites for catalytic fast pyrolysis of biomass and its components. J Anal Appl Pyrol 92(1):224–232

Nguyen MT, Sengupta D, Raspoet G, Vanquickenborne LG (1995) Theoretical study of the thermal decomposition of

acetic acid: decarboxylation versus dehydration. J Phys Chem 99(31):11883–11888
Nimlos MR, Evans RJ (2002) Levoglucosan pyrolysis. Fuel Chem Div Prepr 47(1):393–394
Nowakowski DJ, Bridgwater AV, Elliott DC, Meier D, de Wild P (2010) Lignin fast pyrolysis: results from an international collaboration. J Anal Appl Pyrol 88(1):53–72
Oasmaa A, Elliott DC, Korhonen J (2010) Acidity of biomass fast pyrolysis bio-oils. Energy Fuel 24(12):6548–6554
Ozturk M, Saba N, Altay V, Iqbal R, Hakeem KR, Jawaid M, Ibrahim FH (2017) Biomass and bioenergy: an overview of the development potential in Turkey and Malaysia. Renew Sustain Energy Rev 79:1285–1302
Patwardhan PR, Satrio JA, Brown RC, Shanks BH (2009) Product distribution from fast pyrolysis of glucose-based carbohydrates. J Anal Appl Pyrol 86(2):323–330
Patwardhan PR, Dalluge DL, Shanks BH, Brown RC (2011) Distinguishing primary and secondary reactions of cellulose pyrolysis. Bioresour Technol 102(8):5265–5269
Sacchelli S, De Meo I, Paletto A (2013) Bioenergy production and forest multifunctionality: a trade-off analysis using multiscale GIS model in a case study in Italy. Appl Energy 104:10–20
Shen DK, Gu S (2009) The mechanism for thermal decomposition of cellulose and its main products. Bioresour Technol 100(24):6496–6504
Shen DK, Gu S, Bridgwater AV (2010) Study on the pyrolytic behaviour of xylan-based hemicellulose using TG–FTIR and Py–GC–FTIR. J Anal Appl Pyrol 87(2):199–206
Shen DK, Zhang LQ, Xue JT, Guan SP, Liu Q, Xiao R (2015) Thermal degradation of xylan-based hemicellulose under oxidative atmosphere. Carbohydr Polym 127:363–371
Wang SR, Guo XJ, Liang T, Zhou Y, Luo ZY (2012) Mechanism research on cellulose pyrolysis by Py–GC/MS and subsequent density functional theory studies. Bioresour Technol 104:722–728
Wang SR, Ru B, Lin HZ, Sun WX (2015) Pyrolysis behaviors of four *O*-acetyl-preserved hemicelluloses isolated from hardwoods and softwoods. Fuel 150:243–251
Williams PT, Besler S (1996) The influence of temperature and heating rate on the slow pyrolysis of biomass. Renew Energy 7(3):233–250
Wong MW (1996) Vibrational frequency prediction using density functional theory. Chem Phys Lett 256(4–5):391–399
Zhang XL, Yang WH, Blasiak W (2012) Thermal decomposition mechanism of levoglucosan during cellulose pyrolysis. J Anal Appl Pyrol 96:110–119
Zhang XL, Yang WH, Blasiak W (2013) Kinetics study on thermal dissociation of levoglucosan during cellulose pyrolysis. Fuel 109:476–483
Zhang YY, Liu C, Chen X (2015) Unveiling the initial pyrolytic mechanisms of cellulose by DFT study. J Anal Appl Pyrol 113:621–629